JOURNAL OF THERMOPHYSICS AND HEAT TRANSFER
Vol. 11, No. 3, July–September 1997

Modeling of the Electrogun Metal Vapor Plasma Discharge

Laxminarayan L. Raja,* Philip L. Varghese,† and Dennis E. Wilson‡
University of Texas at Austin, Austin, Texas 78712

The electrogun metal vapor plasma discharge is a new high-power pulsed device for producing vapors of different metals. The process employs electrode erosion to vaporize one of the discharge electrodes. The eroded metal vapor is subsequently ionized to form a dense plasma in which a high current discharge is sustained. The vapor plasma then exits the discharge where it can be used in the synthesis of novel materials or as an ignitor for electrothermal–chemical guns. A model for the electrogun discharge bore plasma flow, bore wall erosion, and simplified models for the cathode and anode regions are presented in this paper. The bore plasma flows under local thermodynamic equilibrium conditions and is weakly nonideal. Two electrogun shots involving different cathode materials (aluminum and titanium) are simulated. Results reveal the physics underlying the operation of the electrogun discharge. High pressures of the bore plasma result in thermal choking at bore exit. Cathode material erosion dominates over the bore wall erosion, thus ensuring a relatively pure metal vapor yield. The exit parameters of the electrogun are predicted and can be used as input boundary conditions for analysis of the external plasma jet flow.

Nomenclature

A_a = anode surface area, m^2
A_b = discharge bore cross section area, m^2
C = capacitance, F
c_s = speed of sound, m/s
d_b = bore diameter, m
d_c = cathode diameter, m
e = electron charge, 1.602×10^{-19} C
e_s = charge state of heavy species s
f = fraction of blackbody radiant energy incident on bore wall
h_{pl} = Planck's constant, 6.6256×10^{-34} J-s
h_0 = total enthalpy, J/kg
I = current, A
J = current density, A/m^2
k_B = Boltzmann constant, 1.3807×10^{-23} J/K
L = external circuit inductance, H
l_b = bore length, m
$\dot{m}''_b$ = mass flux of bore wall erosion, kg/m^2-s
$\dot{m}''_c$ = cathode mass flux, kg/m^2-s
m_e = electron mass, 9.1×10^{-31} kg
n_e = electron number density, m^{-3}
n_i = total ion number density, m^{-3}
n_s = heavy species number density, m^{-3}
n_{tot} = total number density, m^{-3}
p = pressure, Pa
$\bar{Q}_{es}$ = electron–heavy species speed-averaged momentum transfer cross section, m^2
Q_s = internal partition function heavy species s
R_d = discharge resistance, Ω
R_e = external circuit resistance, Ω
R_h = metal vapor gas constant, J/kg-K
r_a = anode radius, m
T = temperature, K
t = time, s
u = plasma mean axial velocity, m/s
V = discharge potential drop, V
x = axial distance from cathode surface, m
Z_{eff} = effective charge on a plasma ion
γ = plasma nonideality parameter
γ_e = correction parameter for electron–electron scattering
$\Delta\varepsilon_{ion,s}$ = lowering of ionization energy of heavy species s, J
$\varepsilon_{ion,s}$ = ionization energy of heavy species s, J
ε_0 = permittivity of free space, 8.854×10^{-12} F/m
ρ = plasma mass density, kg/m^3
σ = electrical conductivity, S/m
σ_{sb} = Stefan–Boltzmann constant, 5.67×10^{-8} W/m^2-K^4

Introduction

THE electrogun is a new device[1] for producing high-speed, high-temperature metal vapor plasma jets using a discharge. The metal vapor plasma can be used in the synthesis of novel materials, especially nanocrystalline ceramics. Additionally, it has been proposed that the electrogun be used as a metal vapor plasma ignitor in electrothermal–chemical guns.[2] The electrogun discharge is a high-power pulsed discharge whose operating parameters are very similar to those of the ablation-controlled capillary plasma devices.[3–6] High-power discharges, whether they operate at high pressures or under vacuum conditions, experience significant erosion of the electrodes.[7] This erosion is normally an undesirable aspect of the discharge and one seeks to minimize this effect. However, the electrogun device relies on the electrode erosion of the discharge as the basic operational phenomenon and is designed to maximize the electrode erosion to obtain the metal vapor yield.[8]

Electrode erosion is perhaps one of the least understood aspects of high-power discharges. Several attempts at understanding this phenomenon have appeared in the literature. Most of these have been with regard to electrode erosion in vacuum arcs[9,10] and in low-pressure (~1 atm) devices[11,12] and rely on the spot theory. However, no comprehensive theory for quantifying the erosion of electrodes in high-pressure (~100 MPa) high-power (~10 MW) discharges exists.

This paper presents an analysis of the electrogun discharge with the primary aim of providing an understanding of the

Presented as Paper 96-2327 at the AIAA 27th Plasmadynamics and Lasers Conference, New Orleans, LA, June 17–20, 1996; received Aug. 12, 1996; revision received Jan. 17, 1997; accepted for publication Jan. 18, 1997.

*Ph.D. Candidate, Mechanical Engineering Department. Student Member AIAA.
†Professor, Department of Aerospace Engineering and Engineering Mechanics. Senior Member AIAA.
‡Associate Professor, Mechanical Engineering Department. Member AIAA.

physics underlying the operation of the discharge. Also, results are obtained for the exit condition of the plasma as a function of the operating parameters of the discharge. These exit conditions are required as input for a separate model that analyzes the plasma jet external to the discharge. The present model gives information that is crucial in the eventual scale-up of the device and should provide insights into electrode erosion phenomena in other high-pressure, high-power devices such as capillary discharges and electromagnetic launchers.

Operation of the Electrogun Discharge

Figure 1 provides a schematic diagram of the electrogun discharge configured to produce a metal vapor plasma jet in a reactor vessel. The reactor vessel, which is nominally at atmospheric pressure, is filled with a suitable gas (nitrogen, oxygen, etc.), such that when the metal vapor plasma mixes, reacts, and condenses in it, it forms nanophase ceramic particles. The electrogun vaporizes a metal by striking an arc between the cathode and an anode. The metal to be vaporized doubles as the cathode and the process relies on cathode erosion. The anode is designed so that its vaporization is negligible.

The electrical energy is stored in the capacitor bank C that is charged to some initial desired voltage, V_{cap}. The pulse-forming network that consists of the capacitor, the inductor L, external resistor R_e, and the resistive load R_d of the discharge provides a pulsed discharge of a few milliseconds duration. A thin metal wire or foil is placed between the cathode and the anode and acts as a fuse that initiates the discharge. The fuse material is the same as the cathode material that is to be vaporized so as to prevent contamination of the product. When the discharge is initiated by an air gap switch $S1$ (Fig. 1), the fuse vaporizes explosively to form the medium for the discharge between the cathode and the anode. The cathode itself then vaporizes and ionizes to sustain a constricted, dense metal vapor arc. The pressure buildup in the discharge bore because of the rapid cathode vaporization then forces the metal vapor plasma into the reactor in the form of a high-speed jet. The plasma then mixes with the gas in the reactor. Finally, the plasma reacts with the gas and condenses to form nanocrystalline particles. The discharge is maintained in this configuration with switch $S1$ closed until the capacitor voltage goes to zero. Switch $S2$ is then closed to short out the capacitor and prevent polarity reversal of the electrodes; the arc extinguishes itself in a few milliseconds.

Electrogun Discharge Analysis: Preliminaries

In this analysis we shall study the results of two individual transients (shots) with separate cathode materials (aluminum and titanium). Parameters of the experimental setup corresponding to these shots are given in Table 1. The geometry of the discharge and the external circuit parameters were the same for the two shots. The differences are in the cathode materials

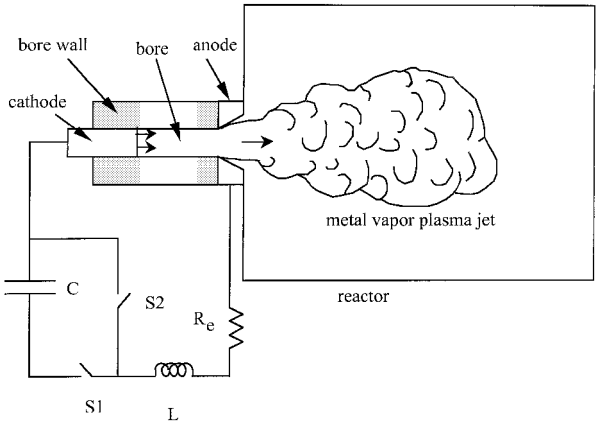

Fig. 1 Schematic diagram of electrogun experimental setup.

Table 1 Electrogun shot parameters

Cathode material	L, μH	R_e, mΩ	C, mF	V_{cap}, kV	d_b, mm	l_b, mm	d_c, mm
Al	23.5	6.5	4.5	8	6.65	13.5	6.65
Ti	23.5	6.5	4.5	5.8	6.65	13.5	6.65

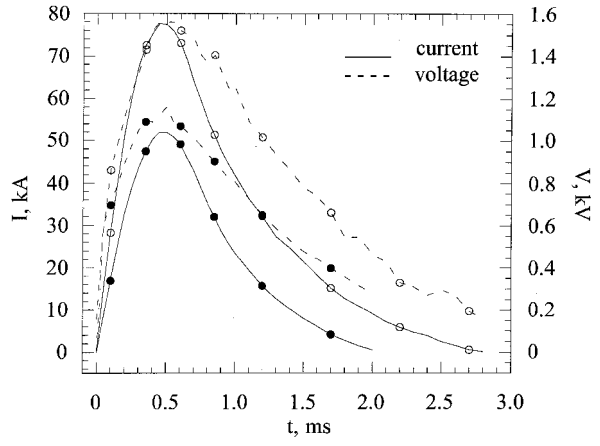

Fig. 2 Transient discharge current and potential drop for Al and Ti shots (open symbols, Al shot; solid symbols, Ti shot).

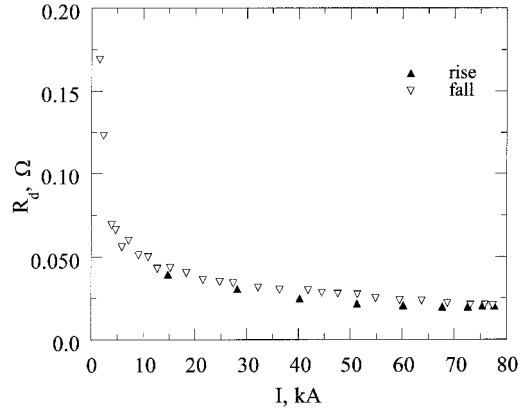

Fig. 3 Experimental discharge resistance data for the Al shot.

and the initial charge voltages of the capacitor bank. Figure 2 shows the transient current and voltage characteristics for the two shots. The single pulse rise and fall in the current and voltage is a consequence of the switching mechanism described earlier. The peak voltage and current for the Ti shot are lower because of the lower initial charge voltage. Analysis of the experimental data for the electrogun shots indicates that the discharge resistance is mainly dependent on the current through the discharge for a given geometry and cathode material. Figure 3 shows the discharge resistance as a function of the current for the aluminum shot. The discharge resistance on the rise and fall portions of the transient fall on a single curve, justifying the previous observation. This indicates that a quasi-steady analysis can be used with the instantaneous current through the discharge as a parameter.

The structure of any discharge can be broadly classified into sheath regions and bulk plasma. The sheaths are adjacent to the solid surfaces such as the electrode and walls, and the bulk plasma region is in the intervening space between the solid surfaces.[13] At high pressures, the sheath regions are extremely thin and their potential drops are negligible compared to the total discharge potential drops and hence can be omitted from the analysis of the discharge. The hydrodynamic flow of the plasma and almost the entire potential drop across the discharge occur in the bulk plasma region. For the electrogun

discharge the plasma exhibits a high degree of ionization with pressures and temperatures of the order of 100 MPa and 30,000 K, respectively. Also, the hydrodynamic flow velocities of the plasma scale with the local speed of sound ($c_s \sim 1$ km/s). A simple estimate

$$l_b/c_s << \left| I \Big/ \frac{\mathrm{d}I}{\mathrm{d}t} \right|$$

indicates that the hydrodynamic time scale is small compared to the time scale for current variation during the discharge pulse. For the pressures and temperatures in the discharge, the molecular time scales for the various processes are negligible compared to the time scale for current variation. These estimates for the hydrodynamic and molecular time scales in the bulk plasma region of the discharge reinforce the quasisteady assumption that was based on the experimental discharge resistance. In the next section we develop a mathematical model for the discharge as a steady-state device whose characteristics vary with the current through the discharge for a given geometry and cathode material. Our analysis will model the discharge for parameters corresponding to the two shots indicated in Table 1. It should, however, be noted that the results are equally valid for any other shot with the same geometry and cathode material.

The high pressures in the device ensure that the electron and heavy species temperatures are described by a single value, despite the high electric fields in the device.[14] Also, the large particle collision rates keep the plasma in a state of thermodynamic equilibrium where the composition and the properties of the plasma are defined by the local state. This is despite the large spatial variations in the properties because of hydrodynamic flow of the plasma. The plasma, however, exhibits nonideal behavior because of high charged particle number densities. The nonideality occurs in that part of the electron number density–temperature parameter space where the interparticle Coulombic potential energy is significant when compared to the particle kinetic energy.[15] This is because of the non-Debye shielding of the Coulomb potential of charged particles at high particle number densities and relatively low temperatures. The nonideality is quantified by the parameter[15]

$$\gamma = \frac{e^2(n_e + n_i)^{1/3}}{4\pi\varepsilon_0 k_B T} \tag{1}$$

Plasmas with $\gamma < 0.1$ are defined as ideal plasmas. For $\gamma \sim 0.1$–1 the plasma is described as weakly nonideal, and for $\gamma > 1$ the plasma is strongly nonideal. For conditions typical of the electrogun discharge the plasma is weakly nonideal.

Electrogun Discharge Analysis: Mathematical Model

The electrogun discharge extends from the cathode surface to the anode surface. It is mathematically convenient to divide the discharge into four regions as follows: the 1) bore plasma, 2) bore wall, 3) anode, and 4) cathode regions. These regions are shown in Fig. 4. The bore plasma region is where the important hydrodynamic phenomena in the discharge occur. This region sets the discharge parameters such as pressure, temperature, and a large part of the discharge potential drop. Also, the high pressures and temperatures of the discharge mentioned earlier are typical of the bore region. The metal vapor eroded from the cathode surface is heated rapidly in the bore via Joule dissipation. The plasma then accelerates axially until it leaves the bore. At the bore exit the plasma encounters pressure conditions typical of the reactor vessel (~1 atm), which causes the flow to be thermally choked.[16] The bore wall region is where ablation of the wall occurs and this material is mixed with the bore plasma flow. The anode region is characterized by the current attachment to the flared anode and the expansion of the plasma after it exits the bore plasma region. In the cathode region the current attachment to the surface occurs in an eroding environment. This region is mathematically an inflow boundary condition to the bore plasma region flow and will be discussed as such.

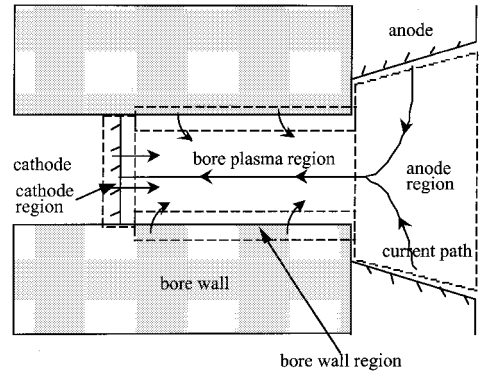

Fig. 4 Schematic description of the physical model regions for the electrogun discharge analysis.

Our analysis here will focus primarily on the bore plasma region because of its importance in setting discharge parameters, especially the cathode erosion rates. This will involve a detailed one-dimensional quasisteady analysis of the hydrodynamic phenomena and a coupling of the plasma hydrodynamic flow with the electric field via the Joule heating source term. The bore wall region will be analyzed in an approximate manner to determine the addition of wall material into the bore plasma flow. An approximate model will also be used to analyze the cathode and anode regions.

Bore Plasma Region

The bore plasma region is similar to that of a capillary plasma discharge. Correspondingly, we use a model for this region that is based on the description of the bore plasma flow of capillary discharges.[4,5] The bulk plasma is modeled as a conducting fluid whose motion through the bore of the discharge is described as a one-dimensional steady flow. The effect of bore wall erosion and the concomitant two dimensionality it lends to the flow is restricted to a thin boundary layer adjacent to the wall. This is shown to be true even for ablation-controlled capillary discharges.[3] Hence, it could be assumed that the ablation products from the bore wall mix nearly instantaneously with the bulk plasma flow and attain mean conditions of the bulk plasma. Also, the conducting plasma is assumed to fill the entire bore cross section.

Flow Equations

The global continuity equation includes external mass addition caused by bore wall erosion and is written as

$$\frac{\mathrm{d}(\rho u)}{\mathrm{d}x} = \sqrt{\frac{4\pi}{A_b}}\, \dot{m}_b'' \tag{2}$$

A model for the bore wall erosion mass flux $\dot{m}_b''$ will be presented later.

The global momentum equation is given by

$$\frac{\mathrm{d}(\rho u u)}{\mathrm{d}x} = -\frac{\mathrm{d}p}{\mathrm{d}x} \tag{3}$$

The previous form assumes that the eroded mass from the bore wall carries zero axial momentum into the bulk plasma. The drag effect of the eroded mass being entrained into the flow appears indirectly through the mass conservation equation. The Lorentz force on the plasma is computed as the cross product between the current density and the magnetic field. Since the

current density in the bore is predominantly axial, the Lorentz force it produces is mainly in the radial direction because of the interaction with the self-induced azimuthal magnetic field. This radial force produces a magnetic pinch pressure that can be shown to be of the order of a few MPa. The pinch pressure itself can be neglected when compared to the discharge thermodynamic pressure. This simplification, along with the thin-wall boundary layer, precludes the need to consider variations in the bore plasma properties in the radial direction. The energy equation includes the convective term and the Joule heating term and is given by

$$\frac{\mathrm{d}(\rho u h_0)}{\mathrm{d}x} = \frac{J^2}{\sigma} \tag{4}$$

The molecular and radiative terms for energy transport in the axial direction are neglected because of the dominant convective transport of energy in that direction. The total enthalpy is given by

$$h_0 = [\tfrac{5}{2} k_B (n_{\mathrm{tot}}/\rho)]T + e_{\mathrm{chem}} + e_{\mathrm{el}} + (u^2/2) \tag{5}$$

The contributing terms listed are the thermal energy, the stored chemical energy associated with vaporization, dissociation, and ionization of the plasma, the electronic excitation energy, and the kinetic energy of the bulk plasma motion, respectively. The lowering of the ionization potential is accounted for in the chemical energy term. The electronic energy is determined by assuming that the populations of various electronic excitation levels of the heavy species are given by the equilibrium Boltzmann distribution. The energy lost by the bulk plasma in ablation of the bore wall is regained as enthalpy of the ablation products. This is because there is negligible heat transfer to the bore wall via conduction since the ablation depths exceed the thermal diffusion depths for the wall material over the time scale of the discharge pulse.

Composition

The composition of the plasma is found as a function of the state of the plasma that is defined by the pressure and temperature. The plasma comprises pure metal eroded from the cathode and the material eroded from the bore wall. In our application the bore wall material is typically an alumina ceramic. The erosion of wall material adds aluminum and oxygen species to the plasma. The bulk plasma is assumed to consist of atoms, ions, and electrons. Up to three ionization levels of the metal atom and two ionization levels for the oxygen atoms are considered. The composition is determined by solving a set of Saha equations representing the generalized law of mass action for ionization and recombination reactions.[14] These equations are of the general form

$$\frac{n_e n_{s+1}}{n_s} = 2\frac{Q_{s+1}}{Q_s}\left(\frac{2\pi m_e k_B T}{h_{\mathrm{pl}}^2}\right)^{3/2} \exp\left[-\frac{(\varepsilon_{\mathrm{ion},s} - \Delta\varepsilon_{\mathrm{ion},s})}{k_B T}\right] \tag{6}$$

where the subscripts s and $s + 1$ indicate the heavy species and their higher ion species, respectively. The partition functions for the monatomic heavy species are determined by considering the degeneracies and energies of the electronic excitation levels.[17] $\Delta\varepsilon_{\mathrm{ion},s}$ is determined for a dense nonideal plasma.[18] The electron number density is found from the quasi-neutrality assumption[14]

$$n_e = \sum_s e_s n_s \tag{7}$$

The equation of state is given by the perfect gas relation

$$p = \left(n_e + \sum_s n_s\right) k_B T \tag{8}$$

It has been shown that deviations from the perfect gas relationship for weakly nonideal plasmas is minimal and can be neglected.[15] The summations in Eqs. (7) and (8) extend over all heavy species.

Transport Properties

Accurate calculation of the electrical conductivity of the plasma is important because it determines the Joule heating of the plasma. For a partially ionized plasma, electron collisions with both neutral atoms and ions determine the electrical conductivity. This is expressed as

$$\sigma = \frac{n_e e^2}{m_e(\bar{\nu}_{\mathrm{en}} + \bar{\nu}_{\mathrm{ei}})} \tag{9}$$

The electron–neutral collision frequency is given by

$$\bar{\nu}_{\mathrm{en}} = \sqrt{\frac{8k_B T}{\pi m_e}} \sum_{s=n} n_s \bar{Q}_{\mathrm{es}} \tag{10}$$

where the summation is over the neutral species in the plasma only. The electron–ion collision frequency is obtained from the Zollweg and Liebermann model for a nonideal plasma[19]

$$\bar{\nu}_{\mathrm{ei}} = \frac{38 Z_{\mathrm{eff}} n_e e^2 \ell n(1 + 1.4\Lambda_m^2)^{1/2}}{\gamma_e m_e T^{3/2}} \tag{11}$$

This model implements a correction to the traditional Spitzer model[20] to account for nonideal effects in a dense plasma. In particular, the nonideal correction has a modified Coulomb parameter Λ_m that includes a modification to the classical Debye shielding cutoff distance for the electron–ion interaction potential.[14] Values for the electron–electron scattering parameter γ_e are obtained from the work of Spitzer and Harm.[21]

Bore Wall Region

A phenomenological model for the bore wall erosion flux is obtained by considering the transmission of radiant energy through the thin boundary layer adjacent to the wall. The dense plasma in the bore is optically thick and the radiation field corresponds to that of a blackbody.[22] Only f is transmitted through the predominantly neutral species boundary layer. The value of f depends on the incident energy flux, the nature of the wall material, and the boundary-layer structure. A simple analysis of the time scale for heat conduction through the bore wall material used in this discharge (alumina ceramic) reveals that no significant heat is transmitted through the wall for the duration of the pulse. Correspondingly, we can assume that the entire energy incident on the bore wall is used in vaporization of the bore material, as mentioned earlier. The bore erosion flux is then given as

$$\dot{m}_b'' = f\sigma_{\mathrm{sb}} T^4 / h_{0_b} \tag{12}$$

where h_{0_b} is the enthalpy of vaporization of the bore wall material. For the conditions appropriate to the present discharge, $f \approx 0.05$.[23] We estimate that $h_{0_b} \approx 30$ MJ/kg for alumina from the bond dissociation energies. This is the same as the method used to estimate the enthalpy of vaporization for plastic materials used in capillary plasma sources.[4]

Anode Region

For capillary discharges, the ring electrode through which the plasma exits the bore is usually flush with the bore, resulting in negligible potential drop in this electrode region. This design is, however, accompanied by erosion of the surface because of the hot flowing plasma. The ring anode of the electrogun is designed for minimum erosion. This is achieved by making the average anode diameter much larger than the bore

diameter to minimize direct contact of the anode with the hot plasma flow. However, this poses a problem for anode arc attachment and there is a corresponding high-potential drop across this region. The experimental potential drop data include the drop in the anode region, and hence, we require a means to compute this value. A simple model for the anode potential drop is derived based on the geometric scales in the anode region and an assumption of uniform current attachment on the anode surface. The anode potential drop is assumed to result from an average current density in the anode region and an effective conductivity of the plasma in this region. The average current density is the algebraic average of the density at the bore exit and the anode surface for the given current. The effective plasma conductivity is some fraction of the conductivity of the plasma at the bore exit because of the rapid expansion and cooling of the plasma in the anode region. The length of the current path in this region is taken as the mean radius of the anode surface. The model gives the anode potential drop as

$$V_a = \kappa(I/\sigma_e) r_a[(1/A_a) + (1/A_b)] \tag{13}$$

Here, σ_e is the conductivity of the plasma at the bore exit. The anode surface area exposed to the flow is given by $A_a = 3.8$ cm^2 with a mean radius of $r_a = 6$ mm. The empirical parameter κ was chosen so that the computed total eroded mass from the cathode is close to the experimental eroded mass for the Al shot. This value was fixed at 0.8 and used for the Ti shot.

Boundary Conditions

The cathode region provides the inlet conditions for the bore plasma region. This inlet condition at the cathode surface is extremely difficult to model for reasons described earlier. In the present study we rely on a simplified approach to treat this region numerically.[8] We assume the cathode surface is spatially uniform and described by a surface temperature T_{cath} with a corresponding saturated vapor pressure P_{cath}. These conditions produce an equilibrium evaporative flux of metal atoms into the bulk plasma. The bulk plasma adjacent to the cathode surface also produces an effusive back-flux of heavy atoms and ions on to the surface. The net mass flux of vapor from the cathode into the bulk plasma is then given by

$$\dot{m}_c'' = (1/\sqrt{2\pi R_h T_{\text{cath}}})(P_{\text{cath}} - P_{h,\text{bulk}}) \tag{14}$$

P_{cath} and T_{cath} are prescribed and are input parameters to the model along with the current density in Eq. (4). In Eq. (14) it is assumed that $T_{\text{bulk}} = T_{\text{cath}}$, where T_{bulk} is the temperature of the plasma adjacent to the cathode surface. $P_{h,\text{bulk}}$ is the heavy particle pressure in the bulk plasma adjacent to the cathode surface and is computed as part of the solution. The boundary condition (14) helps hinge the solution numerically to determine the bore plasma solution uniquely. As mentioned earlier, this artificial boundary condition, with P_{cath} and T_{cath} as parameters, is necessary to circumvent the problem of modeling the actual cathode vaporization process in the presence of the bulk plasma with complex current attachment.

At the exit of the bore the plasma is thermally choked. This implies that the solutions are independent of the conditions in the anode region and the reactor chamber outside the bore. Thus, a linear extrapolation boundary condition is used at the bore exit.

Numerical Solution Procedure

The solution method for the previous equations [Eq. (2–14)] is based on the compressible form of the semi-implicit pressure linked equations (SIMPLE) algorithm.[24] These were solved on a uniform grid of 300 points. A study was conducted to establish that this resolution was sufficient to obtain grid independent results.[8] Since the cathode surface conditions at the inlet to the bulk plasma region are unknown, solutions are obtained for each current level by varying the cathode surface parameters P_{cath} and T_{cath}. This results in varying inlet mass flow rates, and hence, different bulk plasma solutions. Different total plasma potential drops (bore plus anode) are therefore obtained as a part of the solution for different cathode surface parameters. The potential drop can then be compared to the experimentally obtained values to determine realistic input parameters for the model.

Results and Discussion

Figure 5 shows the equilibrium plasma enthalpy for Al vapor plotted as a function of temperature for several pressures. At higher temperatures the enthalpy is dominated by the ionization energy. The ionization regimes for each level of ionization of the plasma species occur over a very broad range of temperature at the high pressures of interest in this study. This causes the enthalpy (and other plasma properties) to vary smoothly with temperature, unlike at lower pressures where distinct jumps occur in the properties in narrow temperature ranges where ionization is dominant.[25] Electrical conductivities are shown on Fig. 6 for the same range of pressures and temperatures. The conductivity increases with temperature at all pressures. At higher pressures the conductivity, like the enthalpy, becomes nearly independent of the pressure and shows only a strong temperature dependence. Although the plasmas considered in this study are a mixture of different species, because of contamination of the plasma from eroded bore wall material, the previous properties for pure metal vapor plasmas are indicative of the general trends in these properties.

Results have been obtained for two different pulsed discharge transients with different cathode materials (see Table 1). The initial voltages of the two shots are different, with the Al shot having a higher capacitor charge. The maximum current level is 80 kA for the Al shot and 50 kA for the Ti shot. Correspondingly, simulations for the two shots are performed

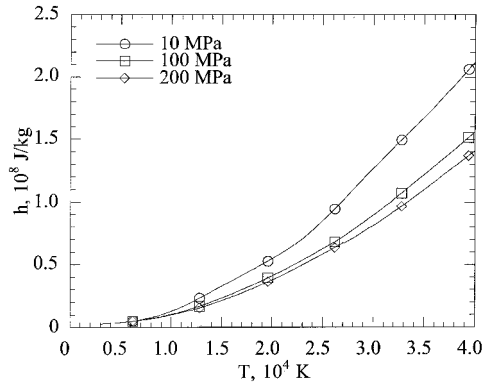

Fig. 5 Equilibrium enthalpy of nonideal aluminum vapor plasma as a function of temperature.

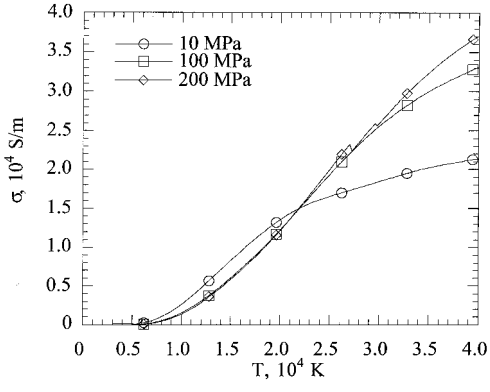

Fig. 6 Electrical conductivity of nonideal aluminum vapor plasma as a function of temperature.

for current parameters up to their respective maximum currents.

Figures 7–9 present results that show the internal structure of the plasma flow in the bore for the two shots considered. Figure 7 gives the axial temperature profiles in the bore of the discharge for different discharge currents. In all cases the temperature rises rapidly over a thin region close to the cathode. This is because of the low electrical conductivity of the plasma close to the cathode surface that results in high Joule heating rates. As expected, the maximum temperatures increase for increasing current levels in the discharge. The temperatures for the Ti discharge are higher than those for the corresponding Al discharge. The slight drop in the temperature as the plasma leaves the bore is because of the rapid expansion of the plasma close to the exit. The titanium shot results are shown only for a maximum current of 50 kA for reasons mentioned earlier. The pressure profiles are shown in Fig. 8. The pressure levels also increase with increasing currents, with higher pressures for the Ti discharge than for the Al discharge. For all cases the pressure drops by a factor of 2 across the length of the discharge. This is typical of standard gasdynamic flows in uniform cross-section pipes with heat addition and thermal choking at the exit.[16] The velocity profiles given in Fig. 9 show trends similar to the pressure and temperature. The maximum velocities at the exit of the bore vary from 4 to 8 km/s for the current levels shown, and the velocities for the Ti discharge are lower than the Al discharge. The exit velocity values are found to be equal to the local speed of sound, confirming the exit choking condition.[16] The differences between the Ti and Al cases at corresponding currents are a reflection of the higher atomic mass of Ti.

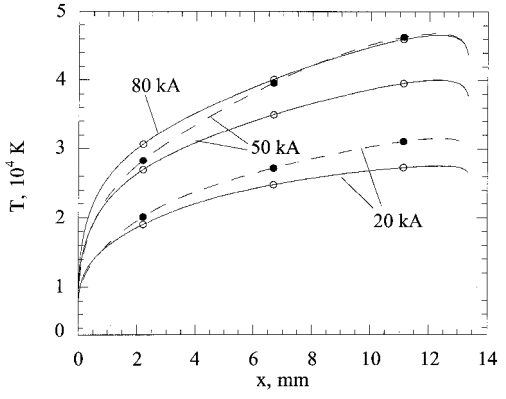

Fig. 7 Electrogun bore plasma temperature variations along the axial direction (open symbols, Al; solid symbols, Ti).

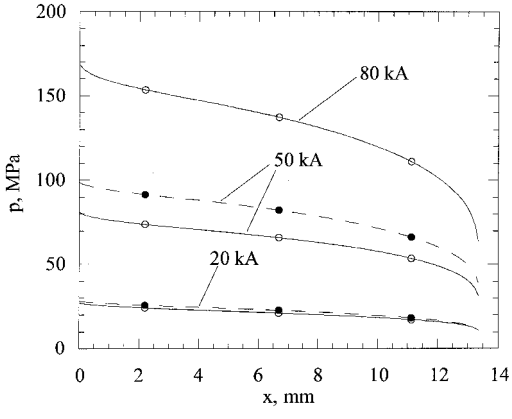

Fig. 8 Electrogun bore plasma pressure variations along the axial direction (open symbols, Al; solid symbols, Ti).

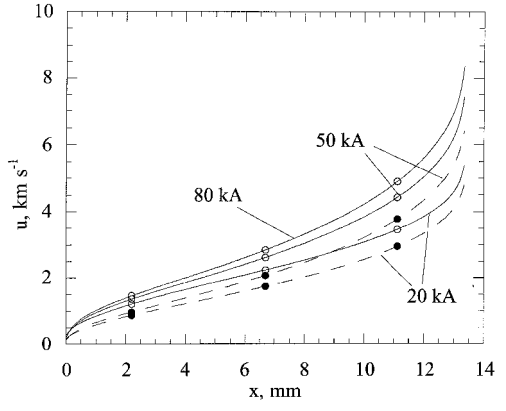

Fig. 9 Electrogun bulk plasma velocity profiles as a function of the axial direction (open symbols, Al; solid symbols, Ti).

The computed erosion rates from the cathode surface and the bore wall for the two materials considered are shown in Fig. 10. Curve fits for the dependence of erosion rates on current are also indicated. Clearly, the bore wall erosion rates are an order of magnitude lower than the cathode erosion rates at all current levels. This confirms that the metal vapor plasma from the cathode is only mildly contaminated by material eroded from the wall. This is because the cathode erosion is influenced by the current attachment in addition to the heat fluxes from the discharge plasma. The cathode erosion rates show a nearly linear dependence on the current level for both the cathode materials as indicated by the curve fits with higher erosion for Ti.

Figures 11 and 12 present the plasma pressure and temperature, respectively, at the bore exit as a function of the discharge current. The Ti plasma shows a higher pressure and temperature for all corresponding current levels. These exit conditions will eventually be used as boundary conditions in simulating the pulsed plasma jet that issues from the discharge

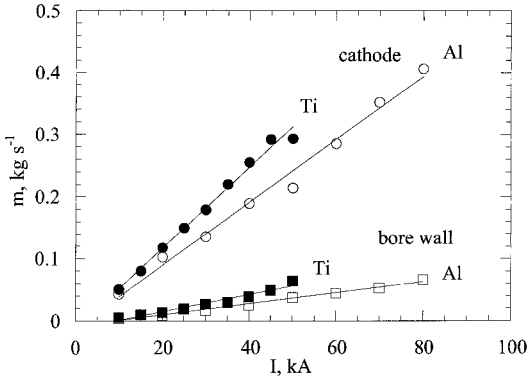

Fig. 10 Computed mass erosion rates from the cathode and bore wall as a function of the discharge current.

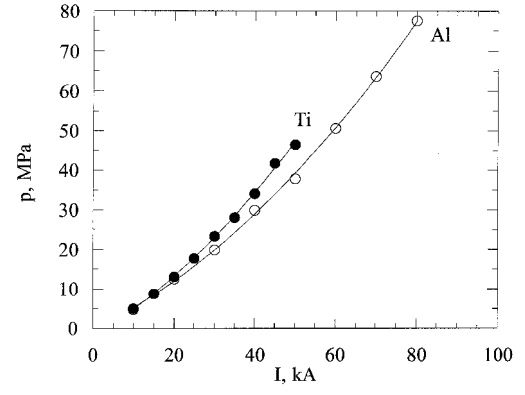

Fig. 11 Bore exit pressures for the Al and Ti cathode discharges as a function of the discharge current.

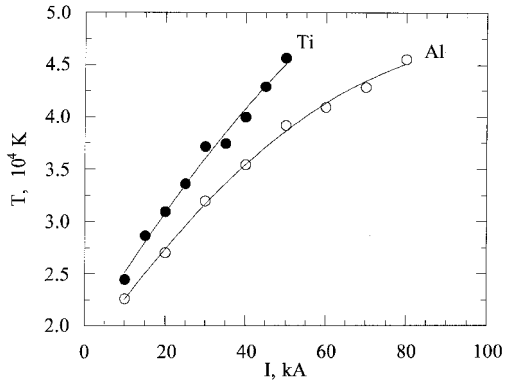

Fig. 12 Bore exit temperatures for Al and Ti cathode discharges as a function of the discharge current.

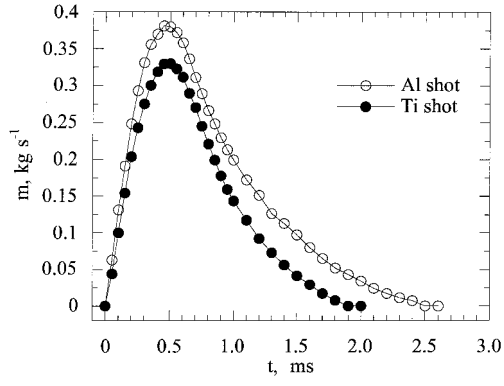

Fig. 13 Transient cathode mass erosion rates.

bore. Curve fits to the previous exit conditions with current as a parameter can be used to determine their transient variation. These variations can be obtained by using the transient current profiles from Fig. 2. The linear curve fits of the cathode mass erosion rates in Fig. 10 are used to determine the transient erosion rates presented in Fig. 13. These curves can be integrated in time to determine the total cathode erosion for the two shots. The computed values for the total cathode erosion are 0.377 and 0.275 g for the Al and Ti shots, respectively. The experimental erosion for the same shots are 0.37 and 0.23 g, respectively. As mentioned earlier, the anode model parameter κ was chosen so that the computed net cathode erosion for the Al shot was close enough to the experimental value. The anode model gave potential drops in the anode region varying from 18% at the lowest current considered to about 22% for the highest currents, in both cases. The computed erosion for the Ti shot is close to the experimental value with a slight overprediction. This overprediction of the net erosion is mainly because of the simplifying assumptions used in the anode model. A more detailed anode model that accounts for the actual physics in this region should provide predictions that are even closer to the experiment. However, the present simple model enables us to obtain reasonable estimates for the erosion and, most importantly, bore exit conditions.

Figure 14 shows the best-fit P_{cath} parameters as a function of the discharge currents for the two cathodes. Under the equilibrium evaporation assumption for which the cathode surface model was developed, P_{cath} represents the true cathode surface pressure. These values are about a factor of 2 higher that the plasma pressure at the cathode surface. Theories available for the electrode erosion phenomena are mostly valid in the range of pressures in which vacuum arcs and atmospheric pressure thermal arcs operate.[9–12] Clearly, the electrogun cathode erosion occurs at much higher pressures and the authors are not aware of any theory that is valid in this regime. It is hoped that the bore plasma results combined with the equilibrium

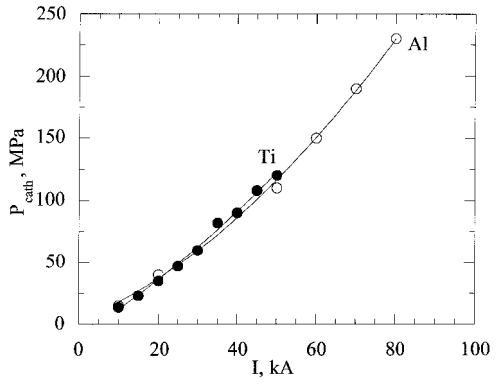

Fig. 14 Best-fit P_{cath} parameters as a function of discharge current for the Al and Ti cathodes.

cathode surface pressures given by P_{cath} will be the basis on which such a theory is developed in the future.

The results presented in this study are found to be sensitive to the model parameters P_{cath} and κ. A study was performed to determine the sensitivity of the model predictions to these parameters.[8] The results showed that a 10% change in P_{cath} from the best-fit values show about 5% change in the discharge potential drops, 19% change in the cathode erosion rates, 9% change in the bore pressures, and about 5% change in the bore plasma velocities and temperatures. The sensitivity of the predictions to the anode model was found by varying κ from its best-fit value that was found from the integrated cathode erosion for the Al shot. Simulations in which the computed and experimental discharge potential drops were matched with about 10% variation in κ, showed about 6% change in the cathode erosion rates, 3% change in the bore pressures, and 2% change in the bore temperatures and velocities. Hence, the plasma temperature and velocities are found to be the least sensitive and the cathode erosion rate the most sensitive to both the parameters P_{cath} and κ.

Conclusions

The electrogun discharge plasma flowfield has been modeled. Based on the time scales for the circuit transient and the discharge processes, a quasisteady assumption seems reasonable for the bulk plasma flow in the bore. The plasma in the bore is at high pressures (~100 MPa) and high temperatures (~30,000 K) that causes it to exhibit weakly nonideal properties under thermodynamic equilibrium conditions. The bore exit is thermally choked causing the bore plasma state to be independent of the external conditions. A parametric model is used for the cathode surface and a simple model is used to determine the potential drops in the anode region. Results for two shots with Al and Ti cathodes reveal the internal structure of the plasma flow in the discharge bore. In general, the Ti cathode shows higher temperatures and pressures and lower axial velocities at corresponding current levels when compared to the Al cathode. The mass erosion rates from the bore wall are an order of magnitude less than erosion from the cathode surface. For all of the surfaces examined (Al, Ti, and alumina) the predicted instantaneous erosion rates are approximately linear with current with somewhat greater scatter for the cathode erosion rates. To our knowledge there is currently no experimental data to test this prediction and such experiments would be very useful to validate the model and provide insight into the mechanisms of surface erosion in this plasma regime. The present model provides initial estimates of the plasma conditions that are necessary for the design of suitable experiments.

Acknowledgment

The authors wish to acknowledge the support for this work from the U.S. Army through the Institute for Advanced Technology at the University of Texas at Austin.

References

[1]Peterson, D., "Electrothermal-Chemical Synthesis of Nanocrystalline Ceramics," Ph.D. Dissertation, Univ. of Texas at Austin, Austin, TX, Dec. 1994.

[2]Raja, L. L., Varghese, P. L., and Wilson, D. E., "Modeling of the Electrogun Ignitor Metal Vapor Plasma for Electrothermal-Chemical Guns," 8th EML Symposium on Electromagnetic Launch Technology, Baltimore, MD, April 1996; also *IEEE Transactions on Magnetics*, Vol. 31, No. 1, 1997, pp. 316–321.

[3]Rutchi, C. B., and Niemeyer, L., "Ablation Controlled Arcs," *IEEE Transactions on Plasma Science*, Vol. PS-14, No. 4, 1986, pp. 423–434.

[4]Gilligan, J. G., and Mohanti, R. B., "Time-Dependent Numerical Simulation of Ablation Controlled Arcs," *IEEE Transactions on Plasma Science*, Vol. 18, No. 2, 1990, pp. 190–197.

[5]Powell, J. D., and Zielinski, A. E., "Theory and Experiment for an Ablating-Capillary Discharge and Application to Electrothermal-Chemical Guns," Ballistic Research Lab., TR-3355, June 1992.

[6]Kovitya, P., and Lowke, J. J., "Theoretical Predictions of Ablation-Stabilized Arcs Confined in Cylindrical Tubes," *Journal of Physics D: Applied Physics*, Vol. 17, No. 6, 1984, pp. 1197–1212.

[7]Jones, G. R., and Fang, M. T. C., "The Physics of High-Power Arcs," *Reports on Progress in Physics*, Vol. 43, No. 12, 1980, 1415–1465.

[8]Raja, L. L., "A Theoretical Model for the Metal Vapor Plasma Discharge of an Electrothermal Gun," Ph.D. Dissertation, Univ. of Texas at Austin, Austin, TX, Dec. 1996.

[9]Ecker, G., "The Vacuum Arc Cathode—A Phenomena of Many Aspects," *IEEE Transactions on Plasma Science*, Vol. PS-4, No. 4, 1976, pp. 218–227.

[10]Rakhovskii, V. I., "Experimental Study of the Dynamics of Cathode Spots Development," *IEEE Transactions on Plasma Science*, Vol. PS-4, No. 2, 1976, pp. 81–102.

[11]Lefort, A., Parizet, M. J., El-Fassi, S. E., and Abbaoui, M., "Erosion of Graphite Electrodes," *Journal of Physics D: Applied Physics*, Vol. 26, No. 8, 1993, pp. 1239–1243.

[12]Durgapal, P., "Electrode Phenomena in High-Current, High-Pressure Arc Heaters," *Journal of Thermophysics and Heat Transfer*, Vol. 7, No. 3, 1993, pp. 412–417.

[13]Pfender, E., "Electric Arcs and Arc Gas Heaters," *Gaseous Electronics*, Vol. 1, Academic, New York, 1978, pp. 291–398.

[14]Mitchner, M., and Kruger, C. H., Jr., *Partially Ionized Gases*, Wiley-Interscience, New York, 1973.

[15]Gunther, K., and Radtke, R., *Electrical Properties of Weakly Nonideal Plasmas*, Birhäuser, Boston, 1984.

[16]Zucrow, M. J., and Hoffmann, J. D., *Gas Dynamics*, Vol. 1, Wiley, New York, 1976, pp. 299–303.

[17]Moore, C. E., "Atomic Energy Levels, Volume I," National Standard Reference Data System, Reprint of NBS Circular 467, Vol. I, 1949, reissued December 1971.

[18]Ebeling, W., and Sandig, R., "Theory of Ionization Equilibrium in Dense Plasmas," *Annalen der Physik*, Vol. 28, 1973, pp. 289–295.

[19]Zollweg, R. J., and Liebermann, R. W., "Electrical Conductivity of Nonideal Plasmas," *Journal of Applied Physics*, Vol. 62, No. 9, 1987, pp. 3621–3627.

[20]Spitzer, L., *Physics of Fully Ionized Gases*, Interscience, New York, 1956.

[21]Spitzer, L., and Harm, R., "Transport Phenomena in Completely Ionized Gas," *Physical Review*, Vol. 89, No. 5, 1953, pp. 977–981.

[22]Batteh, J., Powell, J., Sink, D., and Thornhill, L., "A Methodology for Computing Thermodynamic and Transport Properties of Plasma Mixtures in ETC Injectors," *IEEE Transactions on Magnetics*, Vol. 31, No. 1, 1995, pp. 388–393.

[23]Bourham, M. A., Gilligan, J. G., and Hankins, O. E., "Plasma-Material Interaction in Electrothermal and Electromagnetic Launchers," AIAA Paper 93-3172, July 1993.

[24]Patankar, S. V., *Numerical Heat Transfer and Fluid Flow*, Hemisphere, New York, 1980.

[25]Hansen, C. F., "Molecular Physics of Equilibrium Gases," NASA-SP-3096, 1976.